Water Vapor Feedback in the Tropical Upper Troposphere: Model Results and Observations

KEN MINSCHWANER

Department of Physics, New Mexico Institute of Mining and Technology, Socorro, New Mexico, and Goddard Earth Sciences and Technology Center, Baltimore, Maryland

ANDREW E. DESSLER

Earth System Science Interdisciplinary Center, University of Maryland at College Park, College Park, Maryland

(Manuscript received 16 January 2003, in final form 29 September 2003)

ABSTRACT

The sensitivity of water vapor in the tropical upper troposphere to changes in surface temperature is examined using a single-column, radiative–convective model that includes couplings between the moistening effects of convective detrainment, the drying effects from clear-air subsidence, and radiative heating and cooling from water vapor. Equilibrium states of this model show that as the surface warms, changes in the vertical distribution and temperature of detraining air from tropical convection lead to higher water vapor mixing ratios in the upper troposphere. However, the increase in mixing ratio is not as large as the increase in saturation mixing ratio due to warmer environmental temperatures, so that relative humidity decreases. These changes in upper-tropospheric humidity with respect to surface temperature are consistent with observed interannual variations in relative humidity and water vapor mixing ratio near 215 mb as measured by the Microwave Limb Sounder and the Halogen Occultation Experiment. The analysis suggests that models that maintain a fixed relative humidity above 250 mb are likely overestimating the contribution made by these levels to the water vapor feedback.

1. Introduction

Reducing the uncertainties in predictions of future climate is one of the most pressing issues in atmospheric science today. Projections of surface warmings as large as 5.8°C over the next 100 years are based largely on the expectation of a positive water vapor feedback in the atmosphere (Cubasch et al. 2001). In most global climate models, an initial warming caused by additional CO_2 and other greenhouse gases leads to enhanced evaporation at the surface and a general moistening of the atmosphere. Since water vapor is a strong infrared absorber, the added moisture causes further warming. The amplifying effect can be quite large, increasing the global average warming by 70%–90% compared to calculations that maintain fixed water vapor (Cess et al. 1990).

Observational studies have attempted to verify the positive water vapor feedback by examining the response of atmospheric humidity to changes in surface temperature caused by interannual variability, the annual cycle, volcanic eruptions, and the El Niño–Southern Oscillation (Chou 1994; Sun and Oort 1995; Inamdar and Ramanathan 1998; Blankenship and Wilheit 2001; Soden et al. 2002). Results have been inconclusive, however, with some studies yielding a positive feedback and others indicating a negative response. Aside from the analyses by Soden (1997), Soden and Fu (1995), and Yang and Tung (1998), which examined Television and Infrared Observation Satellite (TIROS) Operational Vertical Sounder (TOVS) mean humidities within a broad layer from 5 to 12 km, none of the empirically based feedback studies focused specifically on humidity in the upper troposphere (UT) of the Tropics (between about 10 and 14 km). It has been pointed out that water vapor radiative effects in this region are important for global climate (Pierrehumbert 1995; Held and Soden 2000).

There are several plausible mechanisms for creating a negative water vapor feedback in the UT (see, e.g., the review by Held and Soden 2000). One oft-cited mechanism invokes the drying effects of deep cumulus convection, arguing that the mean detrainment altitude of deep convection will be both higher and cooler in a warmer climate compared to the present. Because the water vapor content of air pumped into the UT by convection is governed by the saturation vapor pressure at the temperature of cloud detrainment, this would imply

Corresponding author address: K. Minschwaner, Dept. of Physics, New Mexico Institute of Mining and Technology, Socorro, NM 87801.
E-mail: krm@kestrel.nmt.edu

a reduced supply of water at warmer surface temperatures, leading to drying and a negative feedback on climate (Lindzen 1990). Here, we test the convective drying mechanism using a model specifically designed to examine the moisture content of the UT in the Tropics. Implications for the water vapor feedback are also examined using measurements of relative and specific humidities in the tropical UT from microwave and infrared limb-viewing instruments on board the *Upper Atmosphere Research Satellite* (*UARS*; Dessler et al. 1998).

2. Model physics

Over a large fraction (~90%) of the Tropics, tropospheric air experiences a slow subsidence toward the surface. More rapid upward motions within deep convective clouds provide sufficient mass to compensate for this sinking motion. The gentle subsidence of air parcels produces compressional warming, which is balanced by net radiative cooling, a situation that can be approximated within a one-dimensional, radiative–convective framework (Betts and Ridgway 1988; Minschwaner and McElroy 1992; Sun and Lindzen 1993; Sinha and Allen 1994). For the rest of this paper, we will focus exclusively on the nonconvective region. According to this energy balance, the downward flux of mass, M_c, in the nonconvective region is a function of the net radiative cooling, Q_R, and the difference between the ambient lapse rate, $-dT/dz$, and the dry-adiabatic lapse rate, $\Gamma = 9.8$ K km^{-1}:

$$M_c = \frac{Q_R}{c_p\left(\frac{dT}{dz} + \Gamma\right)}, \tag{1}$$

where c_p is the heat capacity of dry air, T is temperature, and z is altitude. Net radiative cooling is controlled to a large extent by the vertical distributions of temperature and humidity:

$$Q_R \simeq Q_R(T, q), \tag{2}$$

where q is the mixing ratio of water vapor. Cooling rates are typically calculated by a numerical model of radiative transfer.

The mean subsidence profile in the present-day Tropics can be calculated using Eqs. (1) and (2), and observed temperatures and humidity (Yanai et al. 1973; Folkins 2002). In general, the subsidence mass flux increases moving downward from the top of convection (~14 km) to about 10 km. Mass conservation requires that this increase in subsidence must be accompanied by a net detrainment of air from deep convection into the free troposphere. If we assume that cloud air detrains from convection fully saturated, and that evaporation of condensate plays a negligible role in this region, then the continuity equation for water vapor is

$$\frac{dM_c}{dz}[q - q^*(T)] = M_c\frac{dq}{dz}, \tag{3}$$

where q and $q^*(T)$ are the mean and saturation water vapor mixing ratios, respectively.

Equations (1), (2), and (3) are tightly interconnected: M_c is a function of Q_R and T, Q_R is a function of q and T, and q is a function of M_c and T. Recent work has shown that the above equations describe the present-day UT well. Folkins et al. (2002) inserted climatological profiles of q and T into Eqs. (1) and (2) to derive the corresponding climatological profile of M_c. This M_c profile was then used in Eq. (3) to derive a q profile. The derived q profile agreed well with the climatological q profile between about 11 and 14 km. This is further confirmed by more sophisticated trajectory models, in which water vapor at pressure levels of 146 and 215 mb—between 11 and 14 km—is well described by detrainment of saturated air and subsequent advection by the large-scale flow (Dessler and Sherwood 2000), and neglecting any contribution from the evaporation of condensate to the mean UT water vapor budget. In the midtroposphere below 10 km, water vapor predicted by Eq. (3) is drier than the observations, suggesting that vertical mixing or evaporation of cloud condensate plays an important role in the middle and lower troposphere (Renno et al. 1994; Folkins et al. 2002).

Solutions to the above three relations, which involve four unknowns (M_c, Q_R, T, and q), require an additional relationship and a boundary condition. Previous studies that used a similar 1D approach to radiative–convective equilibrium employed constraints on M_c, and forced radiative cooling to adjust to the resulting cumulus heating profile (Minschwaner and McElroy 1992; Sun and Lindzen 1993; Sinha and Allen 1994). Here, we adopt constraints on tropical temperatures, relying on the observation that the current tropical atmosphere is nearly moist adiabatic (Xu and Emanuel 1989; Williams et al. 1993) and is expected to remain so over a range of changing surface temperatures (Betts and Ridgway 1992). Given a specified mean surface temperature and relative humidity, the moist pseudoadiabatic profile is calculated. Model temperatures in the convective adjustment region are equal to this moist pseudoadiabat, reduced by a universal profile of buoyancy. The buoyancy profile is symmetric, set to zero at the top and bottom of the convective adjustment region, and reaches a maximum of 4 K at the midpoint.

Temperatures are calculated in this way from the surface upward to the altitude where the radiative equilibrium lapse rate becomes subadiabatic. We define this level to be the top of convection, which closely coincides with the zero net radiative cooling level. Air above this altitude is rising as part of the mean stratospheric circulation; temperatures here are calculated to provide a balance between net radiative heating and dynamical cooling with an ascent rate of 1/40 km day^{-1}, consistent with current estimates of vertical velocities in the trop-

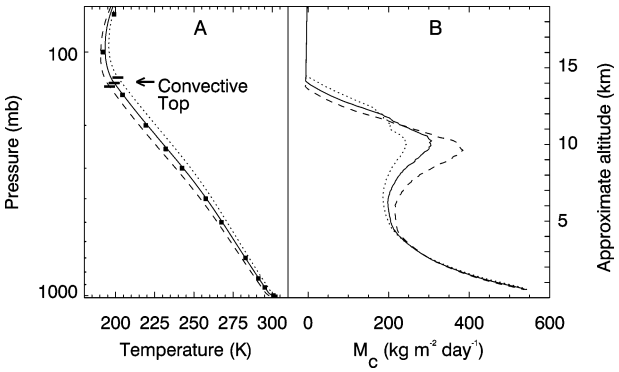

FIG. 1. (a) Model thermal structure for 299-, 301-, and 303-K surface temperatures (dashed, solid, and dotted curves, respectively). Short horizontal lines denote the calculated top of convection. Squares are 1998–2000 means of daily radiosonde observations from Truk, FSM. (b) Calculated rates of clear-air subsidence corresponding to three values of surface temperature.

ical lower stratosphere (Dessler et al. 1996). Rates of radiative heating and cooling [Eq. (2)] throughout the troposphere are calculated using the National Center for Atmospheric Research (NCAR) Community Climate Model 2 (CCM2) radiation model (Briegleb 1992a,b). The model is maintained on a fixed-pressure grid, with 300 levels from the surface to approximately 30 km and a mean layer thickness of 100 m. This fine vertical resolution is necessary to capture small changes in the maximum height of convective detrainment and in vertical gradients of the subsidence mass flux in the UT. Three additional model levels are included to extend the model up to the stratopause.

3. Results

Model temperatures corresponding to three different values of surface temperature and 85% surface relative humidity (Liu et al. 1991) are displayed in Fig. 1. Mean temperatures from Truk, in the Federated States of Micronesia (FSM), which are typical of the Pacific warm pool region, are quite similar to our model case with 301-K surface temperature. We note that the inclusion of dynamical cooling by the Brewer–Dobson circulation is crucial to adequately simulate the height and cold temperature of the tropopause, a problem that has long plagued tropical radiative–convective models (Mahlman 1997). In addition, the calculated convective top appears roughly 2 km below the cold point, similar to observations. The model also shows that increasing surface temperatures lead to a higher and warmer convective top and cold point tropopause.

By specifying details of the profile of M_c, previous radiative–convective model studies of the tropical water vapor feedback did not incorporate the full coupling of Eqs. (1)–(3) into their analyses. In so doing, these models might have missed important responses in the UT to climate forcings. In contrast, our model allows M_c to freely adjust, and instead constrains the temperature profile to remain close to the moist adiabat. The model uses the temperature profiles described above and iteratively solves Eqs. (1)–(3) to produce Q_R, M_c, and q profiles that are consistent with each other and with the temperature distribution over the altitude range between 11 and 14 km. Below this, we assume an exponential increase in the water vapor mixing ratio between the value predicted at 11 km and the lifted condensation level. Stratospheric water vapor is fixed by the calculated temperature of the tropopause (assuming 75% relative humidity at the cold point).

Ozone is another important radiatively active gas, and it is calculated above the top of convection by assuming a balance between production via ultraviolet photolysis of O_2 and upward transport of ozone-poor air from below (Dessler et al. 1996). Tropospheric ozone is determined by the detrainment of air with a value of 20 ppbv, coupled with a net production rate of 1 ppbv day^{-1}. Unless otherwise noted, CO_2 is set to a current mean value of 360 ppmv.

Figure 1 shows how the calculated subsidence flux, which by mass conservation must equal the net upward flux in cumulus convection, responds to changes in surface temperature. As the surface warms, convection penetrates to higher altitudes and the mass flux becomes larger near the top, consistent with larger net rates for radiative cooling in the UT. However, the subsidence rate becomes smaller in the middle troposphere. This result is related to a decrease in temperature lapse rate between about 5 and 10 km, as expected on the basis of a near-moist-adiabatic temperature profile. In addition, the fractional increase in radiative cooling with surface warming is smaller in the middle troposphere in comparison to the UT.

Water vapor profiles are shown in Fig. 2 along with tropical mean observations. As with the case of temperatures and in agreement with Folkins et al. (2002), we find that model UT water vapor with 301-K surface temperature agrees well with the present tropical atmosphere. Our results further show an increasing water vapor mixing ratio as the surface warms, contrary to the convective drying hypothesis. The response seen in our model is the net of two opposing effects. Warming of the UT, in the absence of any other changes, leads to increases in the moisture content of convective detrainment and higher water vapor mixing ratios. In contrast, raising the altitude of detrainment in a fixed temperature profile leads to reduced moisture detrainment and smaller UT mixing ratios. It must be noted that the changes in temperature and detrainment level are linked through Eqs. (1)–(3) and cannot vary independently. Based on our results, warming dominates over higher detrainment, leading to increasing UT water vapor with surface temperature and a positive climate feedback. Clearly, the consistency between M_c, Q_R, and q is an important part of the model, as is the high vertical res-

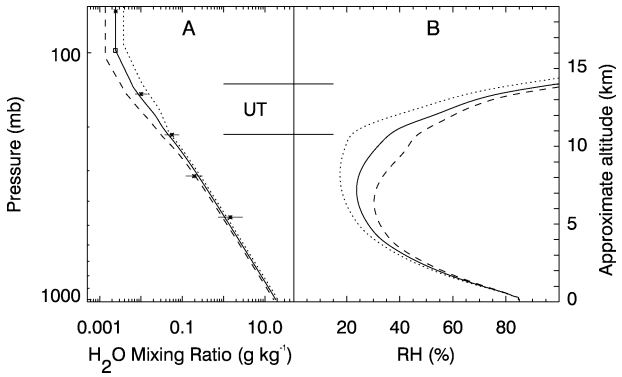

FIG. 2. (a) Model specific humidities for surface temperatures of 299, 301, and 303 K (dashed, solid, and dotted curves, respectively). Data at altitudes below 146 mb are version 4.90 MLS UTH data (Read et al. 2001), averaged between 25°N and 25°S over the period 1992–99. Error bars are based on estimated accuracies. Water vapor at 100 mb represents the annual average H_2O entry value for the stratosphere (Dessler and Kim 1999). Horizontal lines represent the UT layer where water vapor is explicitly calculated. (b) Relative humidities corresponding to the three values of surface temperature.

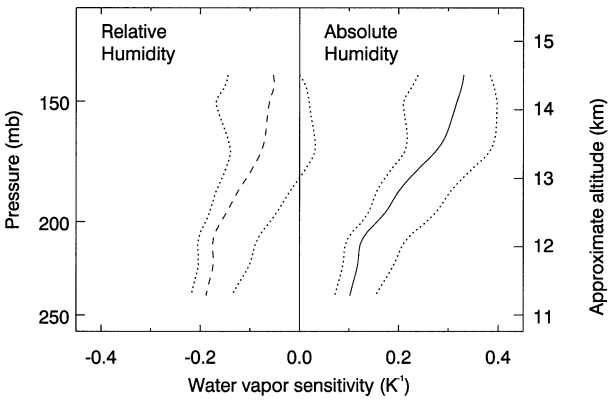

FIG. 3. Sensitivity of relative (dashed) and specific (solid) humidity to changes in surface temperature. Sensitivity is determined by $(dX/X)/dT_s$, where T_s is surface temperature and X is either relative or specific humidity. The dotted curves indicate the maximum possible range of sensitivities through variation of assumed model parameters.

olution required to capture the large gradients in M_c and q in the UT.

The calculated increase in water vapor mixing ratio is not large enough to preserve the relative humidity at a fixed value, as shown in Fig. 2. We find that relative humidity in the UT decreases with increasing surface temperature, on the order of 3%–5% per degree of surface warming. Thus, aspects of the drying mechanisms outlined by Lindzen (1990) are operating in the UT of our model, but not sufficiently to overcome the influence of the Clausius–Clapeyron relation.

Fractional changes in both specific and relative humidities are quantified in Fig. 3. The fractional change in specific humidity increases from 0.1 K^{-1} at the base of the UT to a maximum of about 0.3 K^{-1} near the highest level of convective detrainment. The corresponding fractional changes in relative humidity are -0.2 to -0.05 K^{-1}. A similar trend of decreasing RH with warmer temperature was found by Sun and Oort (1995) using radiosonde observations at altitudes slightly below the UT.

In contrast to these results, the mesoscale model study by Larson and Hartmann (2003) indicated a small increase in UT relative humidity with surface temperature of about +1% RH per degree of warming. The cloud resolving model used by Tompkins and Craig (1999), however, indicated a decrease in relative humidity between 10 and 12 km, which was roughly −2% RH per degree surface warming. The different behavior is likely related to details of the cumulus parameterizations used in these models, which included schemes for simulating high clouds and cloud microphysics. Both models also employed much coarser vertical resolution in the UT, with about four model levels between 11 and 14 km, compared to the ~30 UT levels used in the present study.

The water vapor feedback shown in Fig. 3 is also weaker than that found in a number of general circulation models (GCMs), where relative humidity is found to be nearly invariant throughout the troposphere (Cess et al. 1990; Soden et al. 2002). In comparison to the equilibrium model of the tropical UT presented here, GCMs are confronted with a substantial number of complexities, such as the need to account for surface fluxes, precipitation, evaporation, and long-range transport of water vapor. A detailed discussion of the parameterizations used to represent the physics of moist convection in GCMs is beyond the scope of this paper [some of the more popular schemes are discussed in Emanuel (1994)], and specific causes for the different behavior are difficult to pinpoint. Sun and Held (1996) have postulated that relative humidities in general circulation models may be overly constrained by the strength of vertical mixing that occurs during convective adjustment.

The humidity feedback in our model can also be quantified by the standard measure of response to a doubling of CO_2. In the absence of any change in water vapor, we find a tropical surface warming of 0.8 K for a fixed net radiative flux at the top of the model atmosphere. Inclusion of the feedbacks from Eqs. (1)–(3) produces a larger warming of 1.2 K. Water vapor mixing ratios increase by 20%–50% in the UT, with maximum changes at the top of the model convective outflow near 140 mb (the mean cloud-top level moves up ~200 m in the 2 CO_2 simulation). The vertical profile of change in water vapor is consistent with the GCM feedback study by Colman (2001); however, the magnitude of fractional changes are smaller than the values of 40%–80% found by Colman (2001). On the other hand, maintaining a constant model profile of relative humidity produces larger UT mixing ratio increases, on the order of 60%–75% for doubled CO_2. The stronger water vapor feedback leads to a larger surface warming of 1.6 K, which

TABLE 1. Changes in water vapor sensitivity with variations in model parameters.

	ΔT	α	B–D	Cloud	RH_o	Ice
Max increase (%)	3	10	8	11	4	10
P at max increase (mb)	230	220	200	170	230	200
Max decrease (%)	−4	−5	−3	−11	−9	−2
P at max decrease (mb)	140	230	155	150	145	145

is 30% larger than calculated when relative humidity is not constrained to be constant.

4. Model sensitivities

It is important to note that this is not a study of convective parameterizations, but rather our focus is on the mean state of the larger tropical area in the upper troposphere that is not involved in deep convection. While the details of convective downdrafts, entrainment, and precipitation are clearly important to modeling the tropical atmosphere at the cloud and mesoscale level, here we treat convection as a ''black box'' that impacts the larger tropical domain in three ways, all of which are supported by previous analyses: (i) convection maintains a nearly neutral moist-adiabatic mean temperature, (ii) it provides a net mass detrainment in the UT to balance the flux divergence, and (iii) it detrains saturated air to supply moisture. Nevertheless, our model results may be expected to be sensitive to assumptions regarding the choice of values for certain model parameters, or the neglect of condensate evaporation and the radiative effect of clouds.

Figure 3 includes an estimate of the uncertainty in our results obtained by varying the range of model constraints. While some of these changes produced large differences in the profiles of subsidence mass flux, radiative heating and cooling, ozone mixing ratios, and water vapor, our primary interest is on the net effect of these changes on the calculated water vapor sensitivity, $(dq/q)/dT_s$, shown in Fig. 3. The maximum percent changes in sensitivity with respect to the standard model case are listed in Table 1.

a. Lapse rate

As discussed in section 2, model temperatures are constrained wherever convective adjustment is required by using a universal buoyancy profile referenced to a moist pseudoadiabat. Buoyancy is zero at the lifted condensation level (LCL) and at the convective top (computed in each case to be where the radiative equilibrium lapse rate becomes less than the moist pseudoadiabat). The free parameter is the maximum buoyancy, ΔT, assumed to lie at the midpoint between the LCL and convective top. Our standard model employs $\Delta T = 4$ K, which provides good agreement with the present mean thermal state.

Calculations were also made using $\Delta T = 2$ K and $\Delta T = 8$ K, intended to represent extreme limiting cases in mean convective available potential energy. Since there is a large effect on the temperature lapse rate in the UT, we find that changing ΔT also impacts the calculated subsidence mass flux (by almost a factor of 2) and water vapor mixing ratios (by about 20%). However, changes in the sensitivity of UT water vapor to surface warming $[(dq/q)/dT_s]$ are much smaller (2%–4%). These latter changes are listed in Table 1 (the ΔT column).

b. Middle-tropospheric water

Water vapor mixing ratios in the middle troposphere are determined by interpolating between the amount calculated at the bottom of the UT (about 230 mb), and the input value at the surface (determined by surface temperature and relative humidity). This interpolation assumes $\ln(q) = a \ln(p) + b$, and is designed to implicitly account for moistening effects of shallow convection and evaporation of condensate.

Through the equations of radiative transfer, water vapor mixing ratios in the middle troposphere have a small but non-negligible effect on heating rates in the UT, which may then feed back on subsidence rates and calculated water vapor profiles. We tested this sensitivity by employing two other interpolation schemes that cover a range of extreme distributions in the middle troposphere: $q = ap^{\alpha}$, where $\alpha = 2.7$ or 4.7 (the log–log interpolation in the standard model case is very nearly equivalent to $\alpha = 3.7$). These extremes were equivalent to changing water vapor mixing ratios in the midtroposphere by factors of 2 and 0.5. Corresponding changes in the UT water vapor sensitivity were between 3% and 10% (Table 1, α column).

c. Brewer–Dobson circulation

The strength of upwelling near the tropical tropopause and in the lower stratosphere is important in the thermal equilibrium of these regions. We calculate water vapor based on the temperature of the cold-point tropopause, and model ozone is determined through a balance between vertical transport and photochemical production. Therefore, changes in the model upwelling rate will impact temperature, water vapor, and ozone in the lower stratosphere, leading to changes in radiative cooling rates in the UT as discussed above.

We increased the upwelling rate by a factor of 2, and also reduced the upwelling rate by a factor of 0.5. Very large changes in lower-stratospheric water vapor and ozone were found (up to a factor of 6). The net effect on UT water vapor feedback (Table 1, B–D column) was much smaller.

d. Clouds

Clouds are known to have a large impact on both longwave and shortwave radiation. Our standard cases

assume a clear model atmosphere, which is applicable to a large fraction of the tropical subsiding regions but may not be entirely appropriate for a tropical mean. The largest impact would be on UT cooling rates, which could lead to changes in subsidence and resulting water vapor. To address this possibility, a series of calculations were performed that considered cloudy skies. A 1-km-thick cloud was placed just below the calculated convective top, with cloud fraction of 8% and liquid water path of 3 g m^2. We note that there are practical limits to the magnitude of the radiative heating/cooling perturbation in our model; the simple assumption of subsidence heating balanced by radiative cooling will break down if there is net heating, or if cooling is much greater than a few Kelvins per day.

For the case of cloudy sky, the modeled changes in subsidence mass fluxes and water vapor mixing ratios were up to a factor of 2. Clouds also produced the largest impact on water vapor sensitivity (11%) compared with all of the model changes discussed here (Table 1, cloud column).

e. Surface relative humidity

Table 1 (RH_o column) shows maximum differences in UT water vapor sensitivity for surface relative humidities of 70% and 95%. The standard model assumes 85%.

f. Ice evaporation

Earlier studies have shown that the evaporation of ice does not appear to be important to the overall moisture budget of the UT in the present climate regime (Dessler and Sherwood 2000; Folkins et al. 2002). However, even a small contribution to the humidity budget could impact the magnitude of the calculated feedback. We modified our model by including an additional term in Eq. (3) representing ice evaporation:

$$S_E = \frac{\rho}{\tau}(q^* - q), \tag{4}$$

where S_E is the magnitude of the ice evaporation source and τ is the characteristic time scale for moistening. Values of τ between 1 and 5 days were considered (the standard model assumes an infinite τ). Maximum differences in the water vapor sensitivity were 10% (Table 1, ice column).

The only apparent way to produce a negative feedback in the tropical UT is to assume a large present-day moisture source from evaporation of ice, and then decrease this source to zero as the atmosphere warms. We tested this scenario by including a maximum realistic evaporation source in our present-day model case, with ice evaporation declining to zero at warmer surface temperatures. For the present-day atmosphere, τ can be as short as 2 days and the model will still predict water vapor at the upper limit of observed values. We then assume that τ becomes infinite with a 2-K surface warming. Changes in UT humidity are reduced to nearly zero with this drastic assumption, although the model still fails to produce an overall negative feedback.

5. Observations of UT water vapor

One of the best opportunities to test our model calculations is provided by UT humidity measurements made from the Microwave Limb Sounder (MLS) and from the Halogen Occultation Experiment (HALOE). Both instruments are located on the *UARS* satellite, which was launched in late 1991. In general, both datasets contain a more uniform spatial sampling in the Tropics and higher sensitivity in the UT compared with standard radiosonde observations. We will focus on interannual variations in monthly mean relative and specific humidities, and how these may vary with the mean sea surface temperature (SST) in tropical convective regions.

For MLS, the data used here are upper-tropospheric humidity (UTH) version 4.90 at 215 mb, which span a 5.5-yr period from January 1992 to June 1997. These are relative humidities with respect to ice (% RHi) retrieved from observed limb radiances near 203 GHz (Read et al. 2001). The mean precision of a single measurement at 215 mb in the Tropics is about 15% RHi, and although the microwave observations are relatively unaffected by aerosol, haze, or thin cirrus, there do exist cases where moderately thick cirrus or convective clouds can elevate measurements to values well above 100% RHi. On the other hand, it is clear that supersaturation can occur in the UT (Jensen et al. 1999) and even subsaturated air may produce measured values in excess of 100% due to random errors. The recommended threshold for probable contamination of MLS UT water vapor by clouds is 120% RHi (Read et al. 2001).

We computed monthly mean values of UT humidity between 20°S and 20°N, which encompasses both rising and subsiding branches of the Walker and Hadley circulations, in order to provide a meaningful estimate of the overall tropical feedback (e.g., Lau et al. 1996). Area-weighted averaging was applied to avoid possible biases from uneven spatial sampling. This bias was only an issue for 10% of the months, as most mean values were computed using between 2000 and 10 000 MLS measurements distributed nearly uniformly in latitude and longitude. Even with perfectly uniform sampling, however, there is a possibility for artificial variations arising from month-to-month changes in the number of observations contaminated by cloud. These typically composed between 5% and 10% of the available tropical measurements within any given month, and their spatial distribution correlated well with areas of low monthly mean outgoing longwave radiation (OLR), confirming a high likelihood that these humidities were artificially enhanced by clouds. We therefore excluded measure-

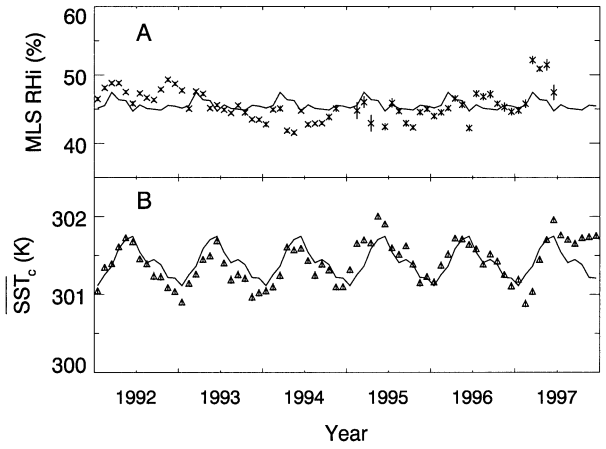

FIG. 4. (a) Monthly mean MLS relative humidity with respect to ice at 215 mb (xs) averaged between ±20° lat. (b) Monthly mean SST (triangles) averaged between ±20° lat and over regions where monthly mean OLR was less than 250 W m^{-2}. Error bars on both sets of data represent the standard error of monthly means (typically 0.5% RHi and 0.05 K, respectively). Solid curves show repeating annual cycles computed from monthly means.

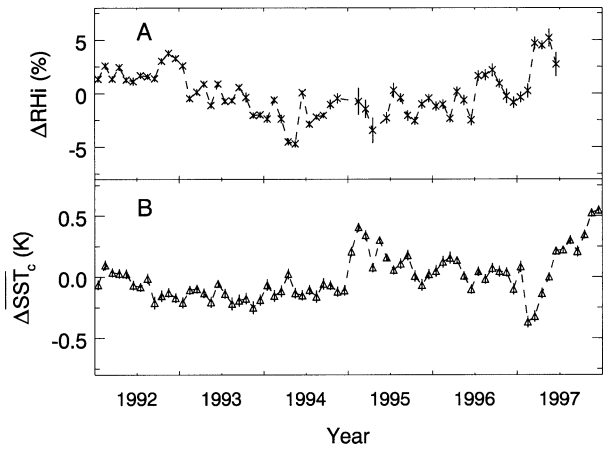

FIG. 5. (a) Monthly mean, deseasonalized MLS relative humidity variations (xs). (b) Deseasonalized SST variations (triangles).

ments greater than 120% RHi so that the monthly means provided a better representation of mean conditions in the subsiding, nonconvective tropical regions simulated by our radiative–convective model.

Figure 4 shows the time series of monthly mean humidity along with the mean seasonal variation computed by averaging over each month of the year. Seasonal means vary between about 44% and 47% RHi, with a clear maximum in March. Note that the model results near 200 mb are in good agreement with this range of values (Fig. 2). Also indicated in Fig. 4 are monthly mean SST, spatially averaged over all areas of the Tropics (±20° latitude) where monthly mean OLR was less than 250 W m^{-2}. These data are designed to represent the mean SST within convective regions of the tropical oceans, $\overline{SST}_c$, which is the surface boundary condition applied to our radiative–convective model. The OLR threshold is based on values (240–260 W m^{-2}) used in previous studies as indices for tropical deep convection (e.g., Waliser et al. 1993). SST was obtained from the (National Centers for Environmental Prediction) NCEP–NCAR 40-Year Reanalysis Project (Kalnay et al. 1996). OLR is from the same dataset, but corrected for diurnal sampling biases from satellite equatorial crossing times (Lucas et al. 2001). The fractional area covered by mean OLR of less than 250 W m^{-2} is typically 30%–35% of the total oceanic area between ±20° latitude. Seasonal $\overline{SST}_c$ means were calculated as above, and these show an amplitude of about 0.6 K with maximum in June.

Interannual variations in RH and $\overline{SST}_c$ are displayed in Fig. 5, which shows differences between each monthly mean and the corresponding seasonal mean. The humidity data show an interannual variability, on the order of 2%–5% RHi, that is larger than the estimated uncertainties computed from the standard deviations of monthly means. Note that the error bars do not include a systematic uncertainty, which is estimated at ±20% RHi. Interannual variations in $\overline{SST}_c$ show indications of the El Niño–Southern Oscillation (ENSO). Peak amplitudes are ±0.5 K, with maxima during the strong 1997/98 and much weaker 1995 El Niño events, and a minimum during the weak 1996/97 La Niña.

As discussed previously, our model calculations predict an overall increase in UT water vapor mixing ratios at warmer surface temperatures, corresponding to a positive feedback situation. Modeled relative humidity shows a small decrease, however, where $[d(\mathrm{RH})/\mathrm{RH}]d(\overline{SST}_c)$ is between −0.10 and −0.21 K^{-1} at 215 mb (Fig. 3). For a mean relative humidity of 40% at 215 mb, this corresponds to a change of −4.0% to −8.4% RHi K^{-1}. A least squares linear fit between the interannual variations in RH and $\overline{SST}_c$ shown in Fig. 5 indicates a weak anticorrelation with a slope of −2.0% ± 3.8% RHi K^{-1}. The linear correlation coefficient is −0.13, which suggests a possible relationship, but in consideration of 64 data points this is not a statistically significant result.

Alternatively, we may expect that the time for equilibrium between changes in $\overline{SST}_c$, boundary layer moist entropy, and convection [on the order of days, e.g., Raymond (1995)], and between convection and the mean relative humidity of the cloud-free Tropics (on the order of weeks—approximately the subsidence timescale in the UT), could lead to phase delays of weeks to a month between $\overline{SST}_c$ and UT humidity. It is hardly surprising, therefore, that we obtain the highest correlation by considering a phase lag of 1 month between UT humidity and $\overline{SST}_c$. Figure 6 shows the relationship between 215-mb humidity and $\overline{SST}_c$ after inclusion of a 1-month phase lag. The least squares regression has an r value of −0.33 and a slope of −4.8% ± 3.4% RHi K^{-1} (2σ uncertainty). No other significant correlations were found for phase relationships between −6 and +6

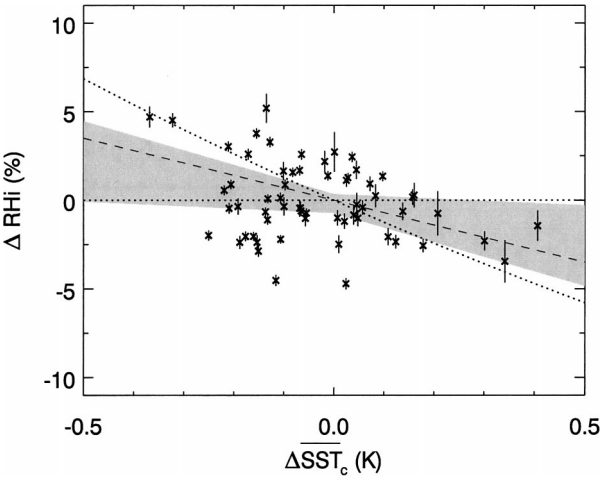

FIG. 6. Relationship between MLS UT relative humidity variations at 215 mb and NCEP SST variations (xs). Data are monthly means between ±20° lat over the period 1992–97 with annual cyles removed, SST means are limited to regions with OLR < 250 W m^{-2}, and a 1-month phase lag is applied between humidity and SST variations. The shaded region is a linear least squares fit with uncertainty (95% confidence limit), the dashed line is the relationship calculated using the radiative–convective model, and the two dotted lines represent the cases of constant relative and specific humidities in the model.

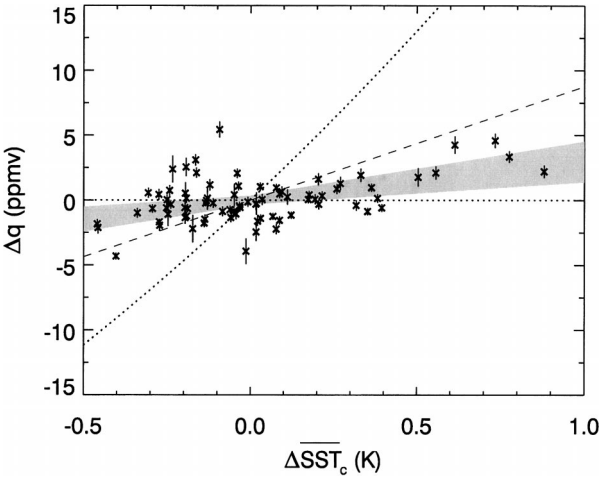

FIG. 7. Relationship between HALOE UT specific humidity variations at 215 mb and NCEP SST variations (xs). Data are monthly means between ±20° lat over the period 1993–99 with annual cycles removed, SST means are limited to regions with OLR < 250 W m^{-2}, and a 1-month phase lag is applied between water vapor and SST variations. The shaded region is a linear least squares fit with uncertainty, the dashed line is the relationship calculated using the radiative–convective model, and the two dotted lines represent the cases of constant specific and relative humidities in the model.

months. In addition, our results indicating a negative slope are relatively insensitive to the choice of OLR threshold for SST averaging. For values between 230 and 270 W m^{-2}, we obtained a range of slopes from -4.0% to -5.1% RHi K^{-1}.

Shown also in Fig. 6 are the results from our model calculations along with two extremes representing a case of constant relative humidity feedback, and the case of zero feedback (constant specific humidity). Despite the large degree of variability and uncertainty in the measured correlation, the observations indicate that the present relationship between tropical-mean UT water vapor and convective-mean SST is constrained between the cases of constant relative and specific humidities, a result that is consistent with the model results presented here. The RH variations in Fig. 6 that appear to be independent of SST could be driven by interannual variations in other variables, such as those discussed in section 4, that are capable of producing perturbations to the mean UT humidity budget.

A similar analysis of water vapor mixing ratios was done using HALOE measurements at 215 mb. These are version 19 data retrieved from observations of solar occultation at infrared wavelengths (Russell et al. 1993). We consider data obtained after 1993 to avoid any impact of volcanic aerosol extinction from the 1991 eruption of Mount Pinatubo. As above, individual measurements were area averaged by month within ±20° latitudes; however, the nature of the HALOE observations does not provide the same number of measurements as for MLS (on the order of 100 as compared to 5000). The monthly averaging period was therefore extended ±10 days to adjoining months, which provided more reliable means with a small smoothing effect on the time series. In addition, the observations are impacted by cloud extinction so that HALOE 215-mb humidities are necessarily biased toward drier tropical regions free from convection and/or cirrus clouds, similar to the Stratospheric Aerosol Gas Experiment II (SAGE II) dataset (Rind et al. 1993). The impact of this bias on the amplitude of observed interannual variations in mean values is difficult to assess, but it could be comparable to the magnitude of the mean dry bias in HALOE water vapor at 215 mb, which is approximately a factor of 2 in comparison with MLS.

Figure 7 shows the correlation between interannual variations in monthly mean UT water vapor and $\overline{\text{SST}}_c$, where the SST variations are computed as before but over the time period 1993–99. As in Fig. 6, we also include the linear least squares fit, model results, and extremes of constant specific and relative humidities. The linear regression shows a positive slope of 3.0 ± 1.2 ppmv K^{-1} (2σ) with a correlation coefficient of 0.47 (80 points). The implied positive feedback is smaller than indicated by our model (8.5–9.5 ppmv K^{-1}), but as with the case of MLS, the HALOE water vapor data show that the UT humidity–$\overline{\text{SST}}_c$ relationship in the present climate regime lies between the cases of constant mixing ratio and constant relative humidity. We also tested the sensitivity of these results to the value of the OLR threshold for SST averaging and consistently found positive correlations varying between 2.6 and 3.1 ppmv K^{-1} for OLR between 230 and 270 W m^{-2}. In addition, removing the six points with $\Delta\text{SST} > 0.5$ K

(resulting from the 1997–98 El Niño) reduced the slope of the regression but still produced a positive value of 1.5 ± 1.7 ppmv K^{-1}.

The variations in tropical UT humidity seen in the MLS and HALOE measurements correspond to certain changes in UT temperature with respect to $\overline{SST}_c$. In particular, since

$$RH = \frac{q}{q^*(T)}, \tag{5}$$

we have that the fractional changes in relative humidity, specific humidity, and saturation humidity are related:

$$\frac{\partial \ln[RH_{215}]}{\partial(\overline{SST}_c)} = \frac{\partial \ln[q_{215}]}{\partial(\overline{SST}_c)} - \frac{\partial \ln[q^*(T_{215})]}{\partial(\overline{SST}_c)}, \tag{6}$$

where the subscript 215 refers to the 215-mb pressure level. The left-hand side of Eq. (6) and the first term on the right-hand side can be inferred from regressions of the MLS and HALOE data as indicated in Figs. 6 and 7: -0.12 and 0.04 K^{-1}, respectively.

The fractional change in saturation mixing ratio is directly related to a change in local temperature. Assuming a saturation mixing ratio given by

$$q^*(T) = q_o^* \exp[-b/T], \tag{7}$$

with $b = 6142$ K (Johnson et al. 2001), we obtain

$$d \ln[q^*(T_{215})] = \frac{b}{T_{215}^2} dT_{215}. \tag{8}$$

Finally, assuming a mean 215-mb temperature of 224 K and using Eqs. (6) and (8), and the regressions in Figs. 6 and 7,

$$\frac{dT_{215}}{d(\overline{SST}_c)} = 1.31, \tag{9}$$

which defines the constraint on interannual UT temperature variations that is implied by the combined MLS–HALOE humidity observations.

This constraint was investigated using 200-mb temperatures archived in the NCEP–NCAR reanalysis (Kalnay et al. 1996). We used the period 1992–99, which overlaps both of the MLS and HALOE observing times analyzed previously. As before, monthly means within $\pm 20°$ latitude were computed with the annual cycle removed to highlight interannual variations. Displayed in Fig. 8 are the 200-mb temperature variations plotted versus $\overline{SST}_c$ variations. A linear regression shows a highly significant correlation ($r = 0.76$) with a slope of 1.44 ± 0.26, a value that is in good agreement with the constraint imposed by MLS–HALOE humidity variations. The above regression is obtained assuming a 1-month phase delay between $\overline{SST}_c$ and T_{215} for consistency with the humidity data presented earlier. However, in this case the regression is insensitive to small changes in timing; a zero-phase regression yields $r = 0.75$ and slope of 1.40, consistent with a more immediate response in mean temperatures compared to mean humidities.

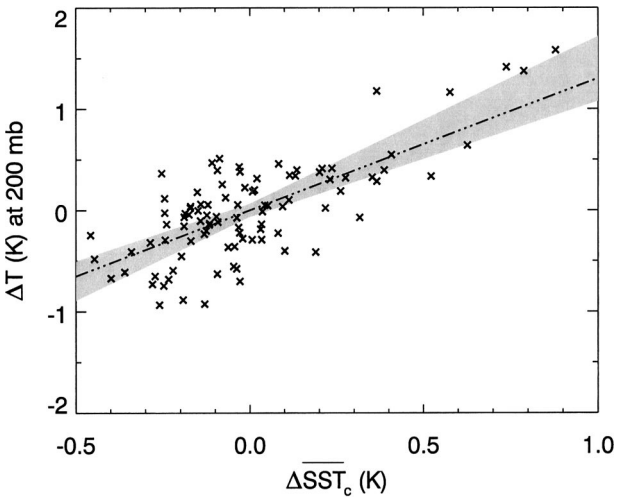

FIG. 8. Relationship between NCEP temperature variations at 200 mb and SST variations (xs). Data are monthly means between $\pm 20°$ lat over the period 1992–99 with annual cycles removed, SST means are limited to regions with OLR < 250 W m^{-2}, and a 1-month phase lag is applied between 200-mb temperature and SST. The shaded region is a linear least squares fit with uncertainty, and the dashed line is the temperature relationship implied by the MLS relative humidity and HALOE specific humidity variations shown in Figs. 6 and 7.

The quantitative agreement between MLS, HALOE, and NCEP data suggests that the feedback is better understood than indicated by the uncertainty in the individual MLS or HALOE fits. The reason is that the MLS and HALOE data are not expected to have any common systematic errors, so that errors in one fit would have to be matched by errors of similar magnitude and sign in the other dataset in order to produce the same result. Such a constraint reduces the uncertainty of the conclusion from the combined dataset.

The MLS and HALOE observations can also be applied individually to compute temperature changes for the limiting cases of constant specific and relative humidities. For the decreasing RH with $\overline{SST}_c$ shown in Fig. 6, an associated zero or negative change in q would correspond to a slope in Fig. 8 that is ≤ 0.98. Alternatively, for the increasing q with $\overline{SST}_c$ in Fig. 7, a case of zero or positive change in RH would correspond to a slope in Fig. 8 that is ≤ 0.33. Both of these situations appear to be ruled out by the temperature variations indicated in Fig. 8. Thus, the change in tropical-mean UT temperature effectively closes the loop on the relative and specific humidity variations seen in the MLS and HALOE datasets.

6. Conclusions

The radiative–convective model described here and applied to the mean state of nonconvecting regions of the Tropics, contains two fundamental constraints that

are almost certain to be applicable to any future climate: a tropical temperature profile that is near moist adiabatic, and a balance in the UT between net radiative cooling, clear-sky subsidence, and the water vapor abundance. The calculated changes in UT water vapor are not dependent on any parameterizations of surface heat and moisture fluxes, and are only weakly impacted by any reasonable assumptions regarding evaporation of cloud condensate. Equilibrium states of the model show that increases in the detrainment height of deep convection and warmer detrainment temperatures lead to increases in the mixing ratio of UT water vapor with increasing surface temperature. The change in water vapor near 215 mb is between 8.5 and 9.5 ppmv K^{-1} increase in surface temperature. On the other hand, the modeled increases in moisture with surface temperature are not enough to preserve constant relative humidity. The calculated decrease in relative humidity at 215 mb is between -4.0% and -8.4% RHi K^{-1}.

Observations of interannual variations in tropical-mean HALOE water vapor and convective-mean SST also support the existence of a positive water vapor feedback in the UT, with an implied moistening of 3.0 $\pm$ 1.2 ppmv K^{-1} at 215 mb. Furthermore, observations of interannual variations in MLS relative humidity and SST show decreases in mean relative humidity with increasing mean SST, on the order of $-4.8\% \pm 3.4\%$ RHi K^{-1}. Both results are consistent with variations in 200-mb temperature and SST from the NCEP–NCAR reanalysis. These observations provide evidence (at the 95% confidence level) that the present climate regime operates between the limiting cases of constant specific and constant relative humidities in the tropical UT. This feedback can be understood in terms of the modeled balance between radiative cooling, clear-air subsidence, and convective detrainment.

The simulated feedback is found to be sensitive to uncertainties arising from possible changes in clouds and lapse rate, and from the evaporation of condensate. One measure of the modeled uncertainty is obtained by varying the range of fixed model parameters used to represent these quantities. We find that the resulting uncertainty is within the limits imposed by current observations of UT humidity and SST. On the other hand, the model can be forced to produce results beyond these limits by artificially changing the cloud amount, lapse rate, and condensate evaporation as the climate changes. Even under the most extreme assumptions regarding these processes, however, we find that the model is unable to produce a negative feedback simulation.

Acknowledgments. The first author acknowledges support through a Goddard Visiting Fellowship in Earth Sciences administered through the University of Maryland, Baltimore County, and hosted by the NASA Goddard Space Flight Center. Other support comes from a NASA EOS/IDS grant and a New Investigator Program grant, both to the University of Maryland. W. Read provided the MLS humidity data used in Fig. 2. We acknowledge useful discussions with I. Folkins, D. Kirk-Davidoff, M. Schoeberl, P. Forster, J. Coakley, P. Newman, S. Sherwood, and W. Read, and beneficial comments from two anonymous reviewers.

REFERENCES

Betts, A. K., and W. Ridgway, 1988: Coupling of the radiative, convective, and surface fluxes over the equatorial Pacific. *J. Atmos. Sci.*, **45,** 522–536.

——, and ——, 1992: Tropical boundary-layer equilibrium in the last ice-age. *J. Geophys. Res.*, **97,** 2529–2534.

Blankenship, C. B., and T. T. Wilheit, 2001: SSM/T-2 measurements of regional changes in three-dimensional water vapor fields during ENSO events. *J. Geophys. Res.*, **106,** 5239–5254.

Briegleb, B. P., 1992a: Delta-Eddington approximation for solar radiation in the NCAR Community Climate Model. *J. Geophys. Res.*, **97,** 7602–7612.

——, 1992b: Longwave band model for thermal radiation in climate studies. *J. Geophys. Res.*, **97,** 11 475–11 485.

Cess, R. D., and Coauthors, 1990: Intercomparison and interpretation of climate feedback processes in 19 atmospheric general-circulation models. *J. Geophys. Res.*, **95,** 16 601–16 615.

Chou, M.-D., 1994: Coolness in the tropical Pacific during an El Niño episode. *J. Climate*, **7,** 1684–1692.

Colman, R. A., 2001: On the vertical extent of atmospheric feedbacks, episode. *Climate Dyn.*, **17,** 391–405.

Cubasch, U., and Coauthors, 2001: Projections of future climate change. *Climate Change 2001: The Scientific Basis*, J. T. Houghton et al., Eds., Cambridge University Press, 525–582.

Dessler, A. E., and H. Kim, 1999: Determination of the amount of water vapor entering the stratosphere based on Halogen Occultation Experiment (HALOE) data. *J. Geophys. Res.*, **104,** 30 605–30 607.

——, and S. C. Sherwood, 2000: Simulations of tropical upper tropospheric humidity. *J. Geophys. Res.*, **105,** 20 155–20 163.

——, K. Minschwaner, E. M. Weinstock, E. J. Hintsa, J. G. Anderson, and J. M. Russell, 1996: The effects of tropical cirrus clouds on the abundance of lower stratospheric ozone. *J. Atmos. Chem.*, **23,** 209–220.

——, and Coauthors, 1998: Selected science highlights from the first 5 years of the Upper Atmosphere Research Satellite (UARS) program. *Rev. Geophys.*, **36,** 183–210.

Emanuel, K. A., 1994: *Atmospheric Convection*. Oxford University Press, 580 pp.

Folkins, I., 2002: Origin of lapse rate changes in the upper tropical troposphere. *J. Atmos. Sci.*, **59,** 992–1005.

——, K. K. Kelly, and E. M. Weinstock, 2002: A simple explanation for the increase in relative humidity between 11 and 14 km in the Tropics. *J. Geophys. Res.*, **107,** 4736, doi:10.1029/2002JD002185.

Held, I. M., and B. J. Soden, 2000: Water vapor feedback and global warming. *Annu. Rev. Energy Env.*, **25,** 441–475.

Inamdar, A. K., and V. Ramanathan, 1998: Tropical and global scale interactions among water vapor, atmospheric greenhouse effect, and surface temperature. *J. Geophys. Res.*, **103,** 32 177–32 194.

Jensen, E. J., W. G. Read, J. Mergenthaler, B. J. Sandor, L. Pfister, and A. Tabazadeh, 1999: High humidities and subvisible cirrus near the tropical tropopause. *J. Geophys. Res.*, **26,** 2347–2350.

Johnson, D. G., K. W. Jucks, W. A. Traub, and K. V. Chance, 2001: Isotopic composition of stratospheric water vapor: Implications for transport. *J. Geophys. Res.*, **106,** 12 219–12 226.

Kalnay, E., and Coauthors, 1996: The NCEP/NCAR 40-Year Reanalysis Project. *Bull. Amer. Meteor. Soc.*, **77,** 437–471.

Larson, K., and D. L. Hartmann, 2003: Interactions among cloud, water vapor, radiation, and large-scale circulation in the tropical climate. Part I: Sensitivity to uniform sea surface temperature changes. *J. Climate*, **16,** 1425–1440.

Lau, K. M., C. H. Ho, and M. D. Chou, 1996: Water vapor and cloud feedback over the tropical oceans: Can we use ENSO as a surrogate for climate change? *Geophys. Res. Lett.,* **23,** 2971–2974.
Lindzen, R. S., 1990: Some coolness concerning global warming. *Bull. Amer. Meteor. Soc.,* **71,** 288–299.
Liu, W. T., W. Tang, and P. P. Niiler, 1991: Humidity profiles over the ocean. *J. Climate,* **4,** 1023–1034.
Lucas, L. E., D. E. Waliser, J. E. Janowiak, P. Xie, and B. Liebmann, 2001: Estimating the satellite equatorial crossing time biases in the daily, global outgoing longwave radiation dataset. *J. Climate,* **14,** 2583–2605.
Mahlman, J. D., 1997: Dynamics of transport processes in the upper troposphere. *Science*, **276,** 1079–1083.
Minschwaner, K., and M. B. McElroy, 1992: Radiative constraints on the energy budget of the tropical atmosphere. *Planet. Space Sci.,* **40,** 1585–1597.
Pierrehumbert, R. T., 1995: Thermostats, radiator fins, and the local runaway greenhouse. *J. Atmos. Sci.,* **52,** 1784–1806.
Raymond, D. J., 1995: Regulation of moist convection over the west Pacific warm pool. *J. Atmos. Sci.,* **52,** 3945–3959.
Read, W. G., and Coauthors, 2001: UARS microwave limb sounder upper tropospheric humidity measurement: Method and validation. *J. Geophys. Res.,* **106,** 32 207–32 258.
Renno, N. O., K. A. Emanuel, and P. S. Stone, 1994: Radiative-convective model with an explicit hydrologic cycle. 1. Formulation and sensitivity to model parameters. *J. Geophys. Res.,* **99,** 14 429–14 441.
Rind, D., E. W. Chiou, W. Chu, S. Oltmans, J. Lerner, J. Larson, M. P. McCormick, and L. McMaster, 1993: Overview of the Stratospheric Aerosol and Gas Experiment II water vapor observations: Method, validation, and data characteristics. *J. Geophys. Res.,* **98,** 4835–4856.
Russell, J. M., and Coauthors, 1993: The Halogen Occultation Experiment. *J. Geophys. Res.,* **98,** 10 777–10 798.
Sinha, A., and M. R. Allen, 1994: Climate sensitivity and tropical moisture distribution. *J. Geophys. Res.,* **99,** 3707–3716.
Soden, B. J., 1997: Variations in the tropical greenhouse effect during El Niño. *J. Climate,* **10,** 1050–1055.
——, and R. Fu, 1995: A satellite analysis of deep convection, upper tropospheric humidity, and the greenhouse effect. *J. Climate,* **8,** 2333–2351.
——, R. T. Wetherald, G. L. Stenchikov, and A. Robock, 2002: Global cooling after the eruption of Mount Pinatubo: A test of climate feedback by water vapor. *Science,* **296,** 727–730.
Sun, D., and R. S. Lindzen, 1993: Water vapor feedback and the ice-age snowline record. *Ann. Geophys.,* **11,** 204–215.
——, and A. H. Oort, 1995: Humidity–temperature relationships in the tropical troposphere. *J. Climate,* **8,** 1974–1987.
——, and I. M. Held, 1996: A comparison of modeled and observed relationships between interannual variations of water vapor and temperature. *J. Climate,* **9,** 665–675.
Tompkins, A. M., and G. C. Craig, 1999: Sensitivity of tropical convection to sea surface temperature in the absence of large-scale flow. *J. Climate,* **12,** 462–476.
Waliser, D. E., N. E. Graham, and C. Gautier, 1993: Comparison of the highly reflective cloud and outgoing longwave radiation datasets for use in estimating tropical deep convection. *J. Climate,* **6,** 331–353.
Williams, E., and N. Renno, 1993: An analysis of the conditional instability of the tropical atmosphere. *Mon. Wea. Rev.,* **121,** 21–36.
Xu, K., and K. A. Emanuel, 1989: Is the tropical atmosphere conditionally unstable? *Mon. Wea. Rev.,* **117,** 1471–1479.
Yanai, M., S. Esbensen, and J. Chu, 1973: Determination of bulk properties of tropical cloud clusters from large-scale heat and moisture budgets. *J. Atmos. Sci.,* **30,** 611–627.
Yang, H., and K. K. Tung, 1998: Water vapor, surface temperature, and the greenhouse effect—A statistical analysis of tropical mean data. *J. Climate,* **11,** 2686–2697.